Research Article Vol. 31, No. 14 / 3 Jul 2023 / Optics Express 23702
Optics EXPRESS

Domain and range of the CIECAM16 forward transformation

CHENG GAO,[1,2] MANUEL MELGOSA,[3] KAIDA XIAO,[4] MICHAEL R. POINTER,[4] AND CHANGJUN LI[2,*]

[1]School of Electronics and Information Engineering, University of Science and Technology Liaoning, Anshan, China
[2]School of Computer and Software Engineering, University of Science and Technology Liaoning, Anshan, China
[3]Department of Optics, University of Granada, Granada, Spain
[4]School of Design, University of Leeds, Leeds, UK
[*]cjliustl@sina.com

Abstract: The domain and range of the CIECAM16 forward transformation was numerically determined and visualized for CIE standard illuminants, using a linear programming approach that provides the gamuts and colour solids for optimum colours. The effect of the surround, adapting luminance, and luminance of the background on the range of the CIECAM16 forward transformation were individually analyzed, showing that their ranges increased when the surround changed from dark to dim or average, the adapting luminance increased, or the luminance of the background decreased. The proposed methodology for the determination and visualization of the domain and range of the CIECAM16 forward transformation can be used for any illuminant, as well as for CIECAM02, CAM16, CAM02-UCS and CAM16-UCS. The findings of this paper not only solve the long-term unresolved domain and range problems of the CIE colour appearance models, but also find applications in cross-media colour reproduction. Furthermore, it was also found that some non-CIE colours are inside the International Color Consortium Profile Connection Space (ICC PCS), and some CIE colours are not included in that space.

1. Introduction

In 2022, CIE recommended CIECAM16 [1], a new colour appearance model for related colours and colour management applications, which replaces CIECAM02 [2]. This new model is mainly based on the CAM16 colour appearance model described by Li et al. [3], with small changes based on the work by Wang et al. [4] and Gao et al. [5]. Like CIECAM02 [2] and CAM16 [3], CIECAM16 [1] also has a forward and an inverse transformation. The CIECAM16 forward transformation can predict colour appearance attributes such as lightness J, colourfulness M, and hue angle h, from the CIE tristimulus values of a sample under the CIE 1931 standard observer and a specified illuminant and surround (i.e. average, dim or dark surround). Unlike CIECAM02, in CIECAM16, both the chromatic and the luminance adaptations are completed in the same CAT16 cone-like space [3]. Hence, CIECAM16 is simpler than CIECAM02, and, in addition, the prediction of visual colour appearance experimental datasets gives performance that is as good or better than that of CIECAM02 [1–3].

Although CIECAM16 solved some problems associated with CIECAM02, such as the so-called "Yellow-Blue" and "Purple" problems [6–8,3], some additional questions related to CIECAM16 are still unsolved. In the clause "Future research" of Ref. [1] four different items were mentioned, the first one being the range of the forward transformation of CIECAM16. In colour management [9,10] both the forward and inverse transformations of CIECAM16 are needed. Furthermore, for efficient colour image reproduction, both transformations on regular grids are used as look up tables and, in a later stage, interpolations are also sometimes needed. In previous colour

#493856 https://doi.org/10.1364/OE.493856
Journal © 2023 Received 28 Apr 2023; revised 12 Jun 2023; accepted 17 Jun 2023; published 30 Jun 2023

Optics EXPRESS

appearance models, such as CIECAM97s [11] and CIECAM02, the domains for the forward and inverse transformations were also unknown. Thus, regular grids were chosen that were large enough to cover these unknown domains. Specifically, the International Color Consortium (ICC) [9] chose regular grids in CIELAB colour space, with L_i^* between 0 and 100, and a_j^* and b_k^* between −128 and 127. When these grids L_i^*, a_j^*, b_k^* are transformed to tristimulus values X, Y, Z, some values were beyond the domain of the CIECAM02 forward transformation [9,10], and this resulted in a problem with computational failure. For CIECAM16, the domain of its forward transformation is all the X, Y, Z values with chromaticity coordinates inside the CIE x, y chromaticity diagram [3]. However, this is too general and further knowledge on the exact boundary or gamut of the domain and range of CIECAM16 would be useful. In fact, investigation into the domains of the forward and inverse transformations started when CIECAM97s was recommended. It is known that the domains and ranges for CIECAM97s, CIECAM02, and CIECAM16 are dependent on the illumination, luminance level and viewing surround. Therefore, there is no way to derive analytical formulae defining such domains and ranges. For the current CIECAM16, it is possible to derive the domain numerically, which is the main objective of this paper.

Note that domain and range are mathematical terms [1]. The domain is a set of one or more variables of a function. For example, if the function is the square of the variable x, the domain of this function is the set of all real numbers. The range of a function is the set of the output of a function for all variables in the domain. Hence, in the previous example, the range is the set of all non-negative real numbers. The range of a function is the domain of the inverse of this function.

2. Boundary of the domain of the forward transformation in CIECAM16

Let Ω_F be the domain of the forward transform in CIECAM16 [1]. The exact definition of Ω_F in a mathematical sense is not important to us. Instead, we search the domain Ω_F which contains all CIE colours, defined as all tristimulus values $X,\ Y,\ Z$ under a given viewing condition, given by

$$\begin{aligned} X &= \kappa \int_a^b E(\lambda) r(\lambda) \bar{x}(\lambda) d\lambda \\ Y &= \kappa \int_a^b E(\lambda) r(\lambda) \bar{y}(\lambda) d\lambda \\ Z &= \kappa \int_a^b E(\lambda) r(\lambda) \bar{z}(\lambda) d\lambda \end{aligned} \quad . \tag{1}$$

where $E(\lambda)$ is the spectral power distribution of the illuminant or light source, $r(\lambda)$ (with values between 0 and 1 for non-fluorescent materials) is the spectral reflectance of the considered sample, $\bar{x}(\lambda)$, $\bar{y}(\lambda)$, and $\bar{z}(\lambda)$ are the CIE 1931 colour-matching functions, and κ is a scaling factor [12] defined by

$$\kappa = 100 / \int_a^b E(\lambda) \bar{y}(\lambda) d\lambda \tag{2}$$

From Eq. (14) of Li et al. [3] it follows that the corresponding values in cone space, $R,\ G,\ B$, are given by

$$\begin{pmatrix} R \\ G \\ B \end{pmatrix} = M_{16} \begin{pmatrix} X \\ Y \\ Z \end{pmatrix} \geq \begin{pmatrix} 0 \\ 0 \\ 0 \end{pmatrix} \tag{3}$$

where M_{16} is the CAT16 matrix [3]. Thus, all $X,\ Y,\ Z$ values in Ω_F defined by Eq. (1) are valid inputs to the forward transformation of CIECAM16.

Optics EXPRESS

In most cases all integrands involved in Eq. (1) have no analytical expressions, hence CIE [12] recommended to replace the integrations in Eq. (1) by 1 nm summations:

$$\begin{aligned} X &= \kappa \sum_{j=1}^{n} E(\lambda_j) r(\lambda_j) \bar{x}(\lambda_j) \\ Y &= \kappa \sum_{j=1}^{n} E(\lambda_j) r(\lambda_j) \bar{y}(\lambda_j) \\ Z &= \kappa \sum_{j=1}^{n} E(\lambda_j) r(\lambda_j) \bar{z}(\lambda_j) \end{aligned} , \tag{4}$$

where,

$$\kappa = 100 / \sum_{j=1}^{n} E(\lambda_j) \bar{y}(\lambda_j). \tag{5}$$

and wavelengths λ_j are uniformly sampled in the visible wavelength range between 380 nm and 780 nm at 1 nm intervals.

Note that for most practical purposes, the summations in Eq. (4) may be approximated by using wavelengths intervals equal to 5 nm over the wavelength range 380 nm to 780 nm [12].

Note also that for $r(\lambda_j) \equiv 1$ the $X,\ Y,\ Z$ values computed using Eqs. (1) or (4) are the tristimulus values of the assumed illuminant (or light source), denoted as X_w, Y_w and Z_w respectively. Since

$$0 \le r(\lambda_j) \le 1 \tag{6}$$

for all non-fluorescent surface colour samples, all $X,\ Y,\ Z$ tristimulus values are located inside a cube with X direction between 0 and X_w, Y direction between 0 and Y_w (= 100), and Z direction between 0 and Z_w. Can we say this cube, denoted as Ω_{XYZ}, is equivalent to Ω_F? The answer has to be no. There are $X,\ Y,\ Z$ values inside this cube that do not represent any CIE colour. In fact, if Y is fixed to be 18.4187, which corresponds to lightness $L^* = 50$, the tristimulus values $X,\ Y,\ Z$ satisfy:

$$\begin{aligned} X &= \kappa \textstyle\sum_{j=1}^{n} E(\lambda_j) r(\lambda_j) \bar{x}(\lambda_j) \\ Y &= \kappa \textstyle\sum_{j=1}^{n} E(\lambda_j) r(\lambda_j) \bar{y}(\lambda_j) = 18.4187 \\ Z &= \kappa \textstyle\sum_{j=1}^{n} E(\lambda_j) r(\lambda_j) \bar{z}(\lambda_j) \end{aligned} . \tag{7}$$

Based on Eq. (7) and inequality (6), Li et al. [13] proposed a linear programming approach to find all proper tristimulus values X and Z and their boundary. It was found by this linear programming approach that the valid tristimulus values X and Z should be enclosed by the dotted curve shown in Fig. 1(a). Thus, this black dotted curve is the boundary or gamut for the tristimulus values X and Z when Y is fixed to a value of 18.4187. It can be considered that the domain enclosed by this dotted curve, together with the fixed Y value, includes all CIE colours. The blue square shown in Fig. 1(a) is the boundary found cutting the cube Ω_{XYZ} by the plane $Y = 18.4187$ assuming CIE illuminant D65 ($X_w = 95.04;\ Z_w = 108.88$). Figure 1(a) shows that many X, Z values enclosed by the blue square are outside the black dotted curve. Thus, in general, many $X,\ Y,\ Z$ values inside the cube Ω_{XYZ} do not represent CIE colours.

Based on the above discussion, when $Y = 18.4187$, the dotted curve shown in Fig. 1(a) can be considered the boundary of Ω_F under CIE illuminant D65. Now, if we sample Y regularly, between 0 and 100, for each Y value, we can find a similar region enclosed by a dotted curve, like the one in Fig. 1(a) in the $X,\ Z$ plane, resulting in the gamut Ω_F under D65. Figure 1(b) shows the gamut Ω_F under D65 with Y set to a value of 1, 5, 10, . . . , 90, 95 and 99, respectively. Hence, sampling in the Y direction is determined first, and next the colour volume or gamut Ω_F as shown in Fig. 1 is obtained. Thus, any regular grid must be on or inside the boundary of this colour volume.

Note that reflectances obtained using the linear programming approach [13] have essentially a mountain-like or a valley-like shape, as shown in Fig. 2. In the literature [14], the former is

Optics EXPRESS

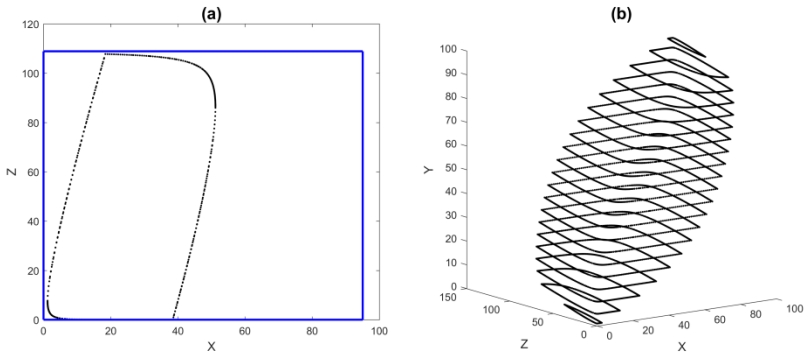

Fig. 1. (a) Black dotted curve: the boundary in X, Z plane when $Y = 18.4187$ under CIE illuminant D65; blue square: the boundary when cutting the cube Ω_{XYZ} by the plane $Y = 18.4187$ under illuminant D65. (b) The gamut Ω_F in X, Y, Z space for $Y = 1, 5, 10, \ldots, 90, 95$ and 99, under illuminant D65.

known as Type 1 reflectance and the latter as Type 2 reflectance. Both types of reflectances provide the so-called 'optimum colours' and are different from the reflectances of real surface colours. Hence, the colour volume or the gamut of Ω_F determined by the proposed approach is called the 'optimum colour solid' [13,14].

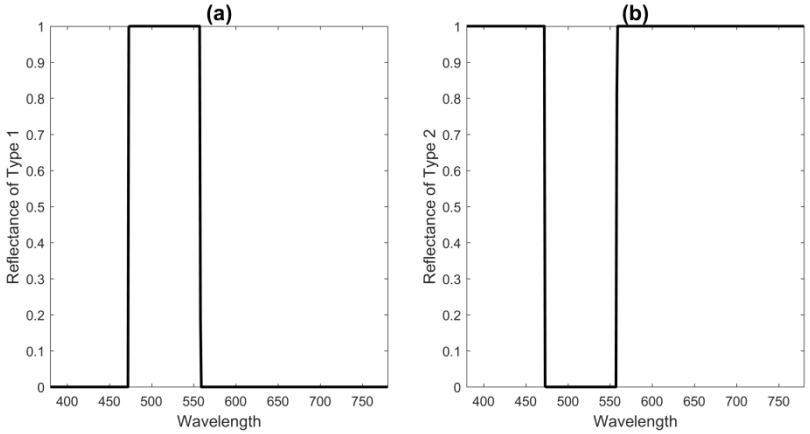

Fig. 2. Reflectance of Type 1 (left) and Type 2 (right) optimum colours.

Since the CIELAB space is more uniform than the XYZ space, it is convenient if the regular grids for Ω_F be defined in the L^*, a^*, b^* space. Figure 3 shows the gamuts (black dotted curves) Ω_F under illuminants C Fig. 3(a) and D50 Fig. 3(b) in the L^*, a^*, b^* space with L^* being set to a value of 1, 5, 10, ..., 90, 95 and 99, respectively. The blue solid curves in Fig. 3(a) and (b) are the real surface colour gamuts from Pointer [15] Fig. 3(a) and ISO [16] Fig. 3(b), respectively. It can be seen that Pointer's gamut is inside the gamut Ω_F, but the ISO gamut is not completely inside the optimum colour solid. Specifically, Fig. 4 shows parts of the blue curves outside the black dotted curve for L^* values of 80, 85, 90 and 95. Thus, the ISO gamut is too large in some regions, which is consistent with the earlier findings of Li et al. [17].

Note that the domain under any illuminant for the forward CIECAM16 can be obtained and visualized using the above approach. The reason to show the domain under illuminant C in Fig. 3(a) is to compare with Pointer's gamut of real surface colours which was defined in terms

Optics EXPRESS

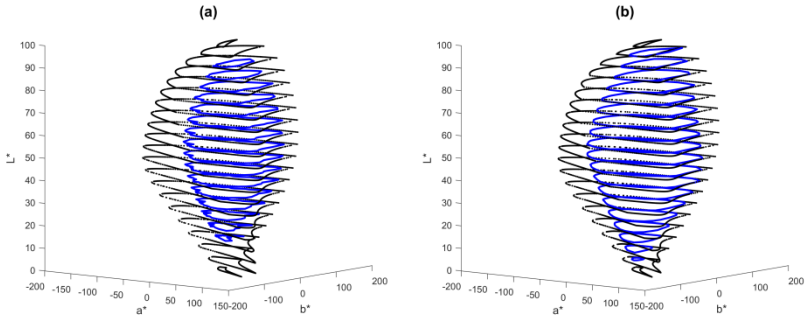

Fig. 3. The black dotted curves are the gamuts (optimum colour solids) Ω_F in L^*, a^*, b^* space under illuminants C (a) and D50 (b) with L^* being 1, 5, 10, . . . , 90, 95 and 99, respectively. The blue solid curves are the real surface colour gamuts from Pointer [15] (a) and ISO [16] (b), respectively.

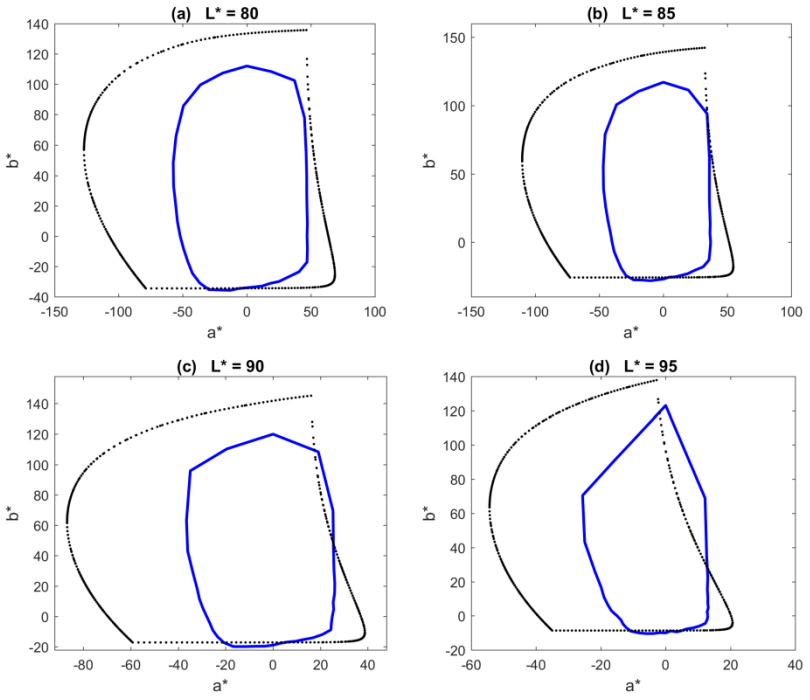

Fig. 4. ISO gamut [15] (blue) and Ω_F (black) in a^* b^* under illuminant D50, for L^* = 80, 85, 90 and 95.

Optics EXPRESS

of L^*, C^*_{ab}, h_{ab} under illuminant C. Similarly, the reason to show the domain under illuminant D50 in Fig. 3(b) is to compare with the ISO gamut of real surface colours and the ICC [9] profile connection space (PCS), which were defined in terms of L^*, C^*_{ab}, h_{ab} and L^*, a^*, b^*, respectively, under illuminant D50.

Note also that ICC [9] defined the PCS, denoted as Ω_{PCS}, in L^*, a^*, b^* space under illuminant D50 with L^* being between 0 and 100, and a* and b* being between −128 and 127. Figure 5 shows Ω_F gamuts in the a^*, b^* plane under illuminant D50 for L^* being 1, 5, 10, . . . , 95 and 99 respectively. The blue square in Fig. 5 is the boundary when cutting the ICC cube Ω_{PCS} by a fixed L* plane in the L^*, a^*, b^* space. It can also be seen that the blue square contains many a^* and b^* values which are not inside the domain enclosed by the black curves, which implies that the ICC cube Ω_{PCS} contains many non-real-world colours. On the other hand, it is interesting to note that, parts of the areas enclosed by the dotted curves are outside the blue square, which may indicate that some real colours are not covered by the ICC cube Ω_{PCS} as well.

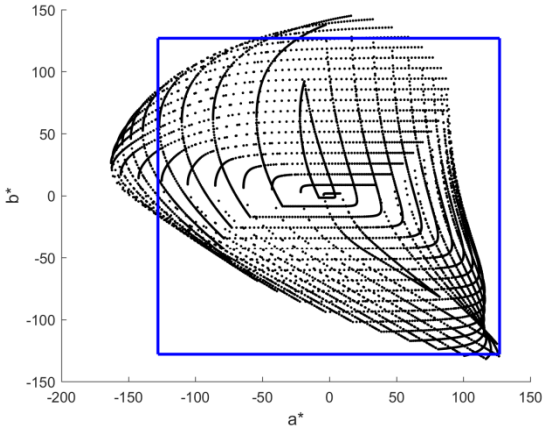

Fig. 5. Gamuts Ω_F in the a^* b^* plane under illuminant D50 with L^* being 1, 5, 10, . . . , 95 and 99 respectively. The blue square is the boundary when cutting the ICC cube Ω_{PCS} by any fixed L^* plane in the L^*, a^*, b^* space.

In summary, the linear programming approach developed by Li et al. [13] is proposed for determining the colour solid Ω_F or domain of the CIECAM16 forward transformation under any viewing condition. Ω_F can be defined in X, Y, Z or L^*, a^*, b^* spaces. Inequality (3) is satisfied for all X, Y, Z in Ω_F. Furthermore, Ω_F covers all real surface colours. Hence Ω_F can be used as the domain for the forward transformation of CIECAM16. The range of the forward transformation or, equivalently, the domain of the inverse transformation of CIECAM16, will be denoted by Ω_R and will be discussed in the next section.

3. Range of the CIECAM16 forward transformation

Determining the domain of the CIECAM16 inverse transformation is equivalent to find the range Ω_R of the forward transformation. In the previous section, we proposed how to compute the domain Ω_F of the forward transformation of CIECAM16 under any illuminant. Thus, the range Ω_R can be determined using the forward transformation, with the appropriate values of surround, background, and adapting luminance, under the specified illuminant. Let the domain Ω_F in X, Y, Z space be determined under CIE illuminant D65 with Y being 1, 5, 10, . . . , 90, 95 and 99, as shown in Fig. 1(b). Figure 6 shows the range Ω_R in J, a_C, b_C space [18] with average surround, $L_A = 40\ \ cd\ m^{-2}$, and $Y_b = 20$.

Optics EXPRESS

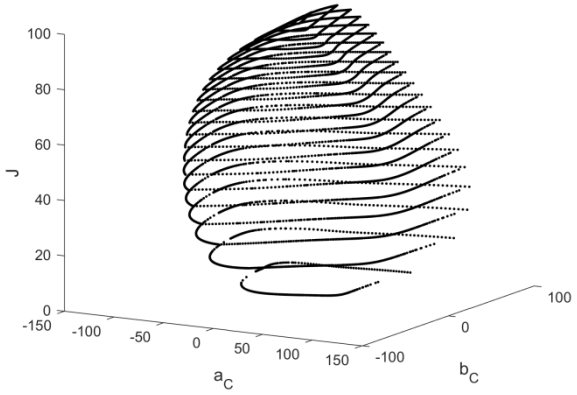

Fig. 6. The gamut or colour solid for the range Ω_R of CIECAM16 in J, a_C, b_C space, using the Ω_F shown in Fig. 1(b) as input, with average surround, $L_A = 40\ cd\ m^{-2}$ and $Y_b = 20$, under CIE illuminant D65.

First, note that any single layer or dotted curve in Fig. 1(b) was transferred to a single dotted curve in J, a_C, b_C space. Thus, as expected, the boundary of the domain Ω_F was transferred to the boundary of the range Ω_R. Second, note that all points in each layer or dotted curve shown in Fig. 1(b) have the same Y value. However, the points on the corresponding layer in the J, a_C, b_C space have different lightness values J, which makes the representation of regular grids in J, a_C, b_C space difficult. To overcome this problem, the convex hull [19] of Ω_R is computed using all points on dotted curves shown in Fig. 6, together with coordinates J, a_C, b_C of the black and white points, obtained using the forward transformation with tristimulus values (0, 0, 0) and $(X_W,\ Y_W,\ Z_W)$ as inputs, respectively. The computed convex hull is shown in Fig. 7. The surface of this convex hull comprises many triangle-shape facets. Note that the colours used in Fig. 7 are only to aid viewing the different triangle-shape facets. It is clear that the intersection of the surface of this convex hull and a plane in J, a_C, b_C space with J being a constant is a closed curve in a_C, b_C space. Figure 8 shows the closed curves obtained using the fixed J plane, with J being 1, 5, 10, . . . , 90, 95 and 99 in J, a_C, b_C space, which may be considered as the gamut of the range Ω_R. The difference between the colour solids shown in Figs. 6 and 8 is that values of lightness J for dotted curves in each layer are different in Fig. 6 and constant in Fig. 8. Hence, it is more appropriate to consider the colour solid shown in Fig. 8 as representative of the range Ω_R of the forward transformation of CIECAM16 (or the domain of its inverse transformation).

Note that a_C, b_C [18] are defined in terms of perceptual attributes chroma C and hue angle h (in degrees) using the following expressions:

$$\begin{aligned} a_C &= C \cdot cos(\pi h/180) \\ b_C &= C \cdot sin(\pi h/180) \end{aligned} \quad . \tag{8}$$

Similarly, a_M, b_M or a_s, b_s can be defined in terms of perceptual attributes colourfulness M and saturation s, respectively. The colour space J, a_C, b_C was considered above. However, depending on the application, other spaces such as J, a_M, b_M or Q, a_C, b_C, can be used.

Now we can summarize the main steps to obtain the gamut and colour solid for the range Ω_R:

Step 1) Determine the gamut of the domain Ω_F under the specified illuminant as discussed in section 2;

Step 2) Obtain boundary points in a colour appearance space, for example J, a_C, b_C, using the forward transformation under specific viewing conditions, which include surround, background,

Optics EXPRESS

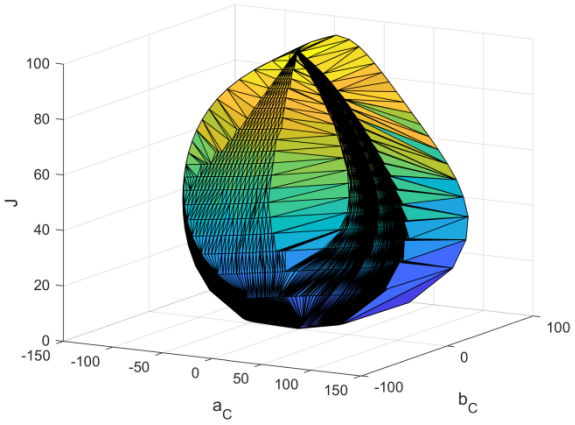

Fig. 7. The convex hull of the range Ω_R shown in Fig. 6.

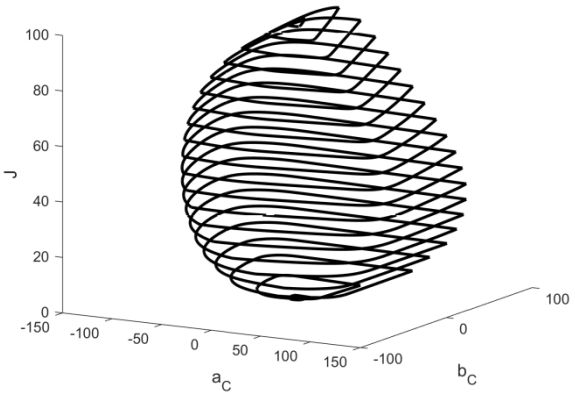

Fig. 8. Gamut and colour solid for the range of CIECAM16 forward transformation in J, a_C, b_C space [18] using the input X, Y, Z shown in Fig. 1(b) with average surround, $L_A = 40\ cd\ m^{-2}$, $Y_b = 20$ under CIE illuminant D65.

and adapting luminance, using as inputs the points on the gamut of the domain Ω_F together with the tristimulus values of the black and white samples;

Step 3) Determine the convex hull using the boundary points obtained in Step 2;

Step 4) Find the intersect closed curves of the convex hull obtained in Step 3 at a series of fixed values of lightness, J (or brightness, Q) planes for the gamut (colour solid) of the range Ω_R.

Based on the above 4 steps, the range Ω_R can be obtained for any illuminant and viewing conditions. As an example, Fig. 9 shows the gamut and colour solid for Ω_R in Q, a_C, b_C space under illuminant D65, average surround, $L_A = 40\ cd\ m^{-2}$ and $Y_b = 20$. Similarly, Fig. 10 shows the gamuts and colour solids for the range of CIECAM16 forward transformation in J, a_M, b_M space with average surround, $L_A = 40\ cd\ m^{-2}$, $Y_b = 20$ under illuminants D65 Fig. 10(a), D50 Fig. 10(b) and A Fig. 10(c), which are the three standard illuminants currently adopted by the CIE.

Based on the determined range Ω_R, the influence of the surround, adapting luminance level and background can be further investigated. Figure 11 shows the gamut of Ω_R in a_M, b_M space when J is fixed to 50 for average (black curve), dim (blue curve) and dark (red curve) surrounds, under illuminants D65, D50 and A. In Fig. 11 the values of the adapting luminance and background were $L_A = 40\ cd\ m^{-2}$, $Y_b = 20$, as used in Fig. 10. It can be noted that the areas covered by the

Optics EXPRESS

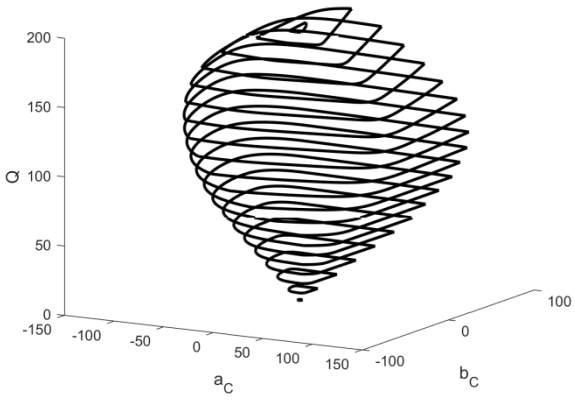

Fig. 9. Gamut and colour solid for the range of CIECAM16 forward transformation in Q, a_C, b_C space using the input X, Y, Z values shown in Fig. 1(b) with average surround, $L_A = 40\ cd\ m^{-2}$, $Y_b = 20$ under illuminant D65.

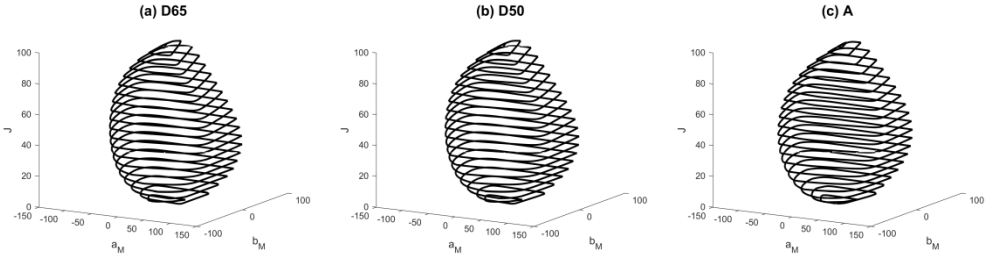

Fig. 10. Gamuts and colour solids for the range of CIECAM16 forward transformation in J, a_M, b_M space with average surround, $L_A = 40\ cd\ m^{-2}$, $Y_b = 20$ under CIE illuminant D65(a), illuminant D50 (b) and illuminant A (c).

black/red curves are the largest/smallest, which confirms the expectation that the volumes of the gamuts [20–22] decrease when we change from average to dim and dark surround. Figure 12 shows the gamut of Ω_R in a_M, b_M space when J is fixed to 50 for $L_A = 10\ cd\ m^{-2}$ (green curve), $50\ cd\ m^{-2}$ (magenta curve), $100\ cd\ m^{-2}$ (middle grey curve) with average surround, $Y_b = 20$, under illuminants D65 Fig. 12(a), D50 Fig. 12(b) and A Fig. 12(c). It can be noted that with larger L_A values the area enclosed by the curve increases, which is consistent with the Hunt effect [22]. Figure 13 shows the gamuts for the range of CIECAM16 forward transformation in a_M, b_M space, when J is fixed to 50, with average surround, $L_A = 40\ cd\ m^{-2}$, and $Y_b = 5$ (cyan curve), 20 (black curve) and 50 (yellow curve), under illuminants D65 Fig. 13(a), D50 Fig. 13(b) and A Fig. 13(c). It can be noted that when Y_b is smaller, the area enclosed by the curve is larger, which is consistent with the lightness contrast and Hunt effects [22,23]. The lightness contrast effect tells us the perceived lightness increases when colours are viewed against a darker background. Then, from Hunt effect, the lighter colours appear more colorful. Hence, in Fig. 13 the areas enclosed by the black/red curves are the largest/smallest.

Finally, we can add that the domain Ω_F for the CIECAM16 forward transformation is also the domain for CIECAM02 and CAM16. In fact, in Ref. [24] the robustness of CIECAM02 was tested using the domain Ω_F. The range Ω_R for CIECAM02 and CAM16 forward transformations can be determined in a similar way to that for CIECAM16. The proposed methodology can be also used to determine and visualize ranges in the CAM16-UCS [3] and CAM02-UCS [12,25] uniform colour spaces.

Optics EXPRESS

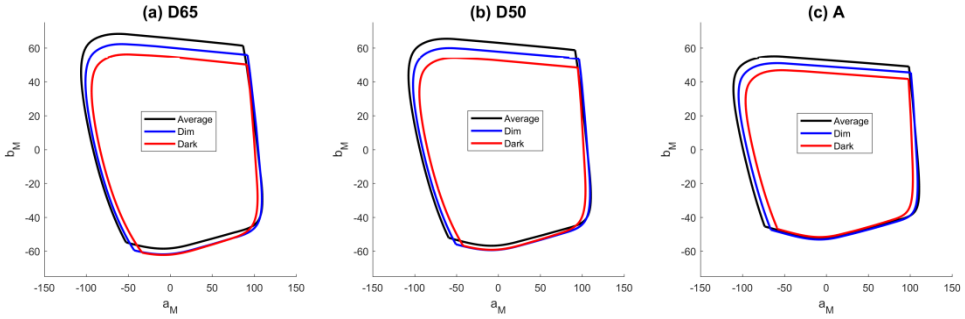

Fig. 11. The gamuts for the range of CIECAM16 forward transformation in a_M, b_M space, when J is fixed to 50, for average (black curve), dim (blue curve) and dark (red curve) surrounds, $L_A = 40\ cd\ m^{-2}$, $Y_b = 20$, under illuminants D65 (a), D50 (b) and A (c).

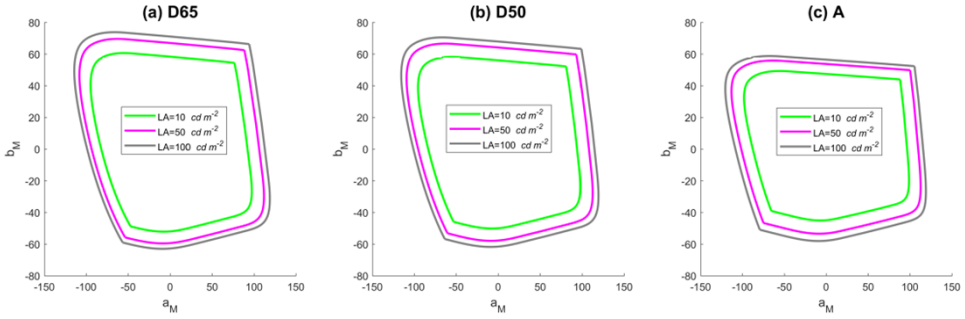

Fig. 12. The gamuts for the range of CIECAM16 forward transformation in a_M, b_M space, when J is fixed to 50, with average surround, $Y_b = 20$, and $L_A = 10\ cd\ m^{-2}$ (green curve), 50 $cd\ m^{-2}$ (magenta curve) and 100 $cd\ m^{-2}$ (middle grey curve), under illuminants D65 (a), D50 (b) and A (c).

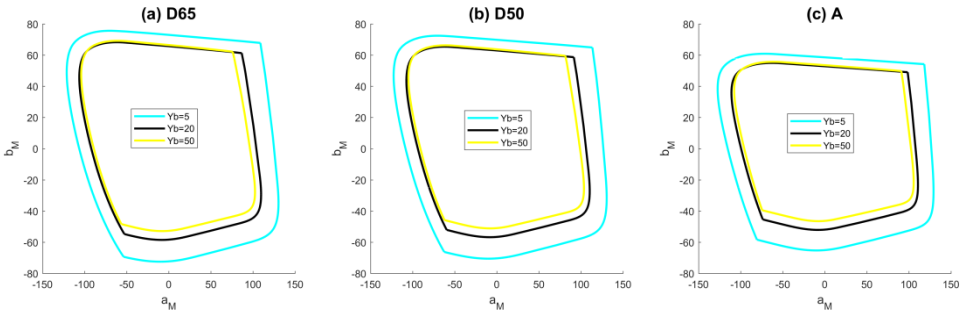

Fig. 13. The gamuts for the range of CIECAM16 forward transformation in a_M, b_M space, when J is fixed to 50, with average surround, $L_A = 40\ cd\ m^{-2}$, and $Y_b = 5$ (cyan curve), 20 (black curve) and 50 (yellow curve), under illuminants D65 (a), D50 (b) and A (c).

Optics EXPRESS

4. Conclusions

CIE has recommended a new colour appearance model, CIECAM16 [1], to replace CIECAM02 [2]. Unlike CIECAM02, in CIECAM16 the chromatic and luminance adaptations are completed in the same CAT16 cone-like space [3]. Hence, CIECAM16 is simpler than CIECAM02, and the performance of CIECAM16 in predicting visual colour appearance datasets is as good as or better than that of CIECAM02 [3]. However, in Ref. [1] four unsolved problems were identified, the first being the range of the forward transformation which has been analyzed in the current paper.

In this paper, first the domain Ω_F of the forward transformation under any illuminant was numerically determined and visualized using the linear programming approach in Ref. [13] to find the gamut and colour solid of the optimum colours [12]. Second, the gamuts and colour solids of the ranges Ω_R of the CIECAM16 forward transformation under different viewing conditions were determined and visualized using the identified domain Ω_F. The ranges Ω_R can be represented in different colour spaces such as J, a_M, b_M or J, a_C, b_C, or Q, a_C, b_C, depending on the application. Finally, the effects of the surround, adapting luminance level, and background were investigated separately, showing ranges Ω_R for three standard CIE illuminants (D65, D50 and A). It was found that the ranges increase when the surround changes from dark to dim and average, and also that ranges increase with the increase of the adapting luminance or the decrease of the luminance of the background.

The proposed methodology for determining and visualizing the domain and range of the CIECAM16 forward transformation can be also applied to determine those for CIECAM02, CAM16, CAM02-UCS and CAM16-UCS. The analysis and results reported in this paper provide a solution to one of the long-term unresolved domain and range problems of the CIE colour appearance models, and will have application in cross-media colour reproduction.

Furthermore, it is shown that part of the ICC PCS Ω_{PCS} under CIE illuminant D50 is outside of the domain Ω_F (see Fig. 5), which implies that the ICC PCS cube Ω_{PCS} contains non-CIE (i.e. unreal) colours. It is also shown that some X, Y, Z values locate inside Ω_F, but outside Ω_{PCS}. (see Fig. 5), which implies that some CIE colours are not covered by the ICC PCS.

Funding. National Natural Science Foundation of China (61575090, 61775169); Department of Education of Liaoning Province (LJKQZ2021127, LJKZ0291, LJKZ0310); University of Science and Technology Liaoning (2021YQ04, LKDYC202103); Ministerio de Ciencia e Innovación (PID2019-107816GB-I00/SRA/10.13039/501100011033).

Disclosures. The authors declare no conflicts of interest.

Data Availability. Data underlying the results presented in this paper are not publicly available at this time but may be obtained from the authors upon reasonable request.

References

1. CIE 248:2022, *The CIE 2016 colour appearance model for colour management systems: CIECAM16*, (CIE Central Bureau, Vienna, 2022).
2. CIE 159:2004, *A colour appearance model for colour management systems: CIECAM02*, (CIE Central Bureau, Vienna, 2004).
3. C. J. Li, Z. Q. Li, Z. F. Wang, Y Xu, M. R. Luo, G. H. Cui, M. Melgosa, M. H. Brill, and M. R. Pointer, "Comprehensive color solutions: CAM16, CAT16 and CAM16-UCS," Color Res. Appl. **42**(6), 703–718 (2017).
4. Z. F. Wang, C Gao, Y Xu, M. Melgosa, M. H. Brill, M. R. Pointer, and C. J. Li, "Further investigation on the modified hyperbolic function in the CAM16 color appearance model," Color Res. Appl. **44**(3), 359–366 (2019).
5. C Gao, Z. F. Wang, Y Xu, M. Melgosa, K. D. Xiao, M. H. Brill, and C. J. Li, "The von Kries chromatic adaptation transform and its generalization," Chin. Opt. Lett. **18**(3), 033301 (2020).
6. M. H. Brill, "Irregularity in CIECAM02 and its avoidance," Color Res. Appl. **31**(2), 142–145 (2006).
7. M. H. Brill and S. Süsstrunk, "Repairing gamut problems in CIECAM02: A progress report," Color Res. Appl. **33**(5), 424–426 (2008).
8. J. Jiang, Z. F. Wang, M. R. Luo, M. Melgosa, M. H. Brill, and C. J. Li, "Optimum solution of the CIECAM02 yellow-blue and purple problems," Color Res. Appl. **40**(5), 491–503 (2015).
9. I. Tastl, M. Bhachech, N. Moroney, and J. Holm, "ICC Color Management and CIECAM02," in *13th Color and Imaging Conference (CIC)* (2005), pp. 217–223.
10. R. Guay and M. Shaw, "Dealing with Imaginary Color Encodings in CIECAM02 in an ICC Workflow," in *13th Color and Imaging Conference (CIC)* (2005), p. 318.

Optics EXPRESS

11. M. R. Luo and R. W. G. Hunt, "The structure of the CIE 1997 colour appearance model (CIECAM97s)," Color Res. Appl. **23**(3), 138–146 (1998).
12. CIE 015:2018, *Colorimetry*, 4th edition, (CIE Central Bureau, Vienna, 2018).
13. C. J. Li, M. R. Luo, M-S Cho, and J-S. Kim, "Linear programming method for computing the gamut of object color solid," J. Opt. Soc. Am. A **27**(5), 985–991 (2010).
14. F. Martínez-Verdú, E. Perales, E. Chorro, D. de Fez, V. Viqueira, and E. Gilabert, "Computation and visualization of the MacAdam limits for any lightness, hue angle and light source," J. Opt. Soc. Am. A **24**(6), 1501–1515 (2007).
15. M. R. Pointer, "The gamut of real surface colours," Color Res. Appl. **5**(3), 145–155 (1980).
16. ISO 12640-3:2007, "Graphic technology - Prepress digital data exchange – Part 3: CIELAB standard colour image data (CIELAB/SCID)," ISO, 2007.
17. C. J. Li, M. R. Luo, M. R. Pointer, and P. Green, "Comparison of real colour gamuts using a new reflectance database," Color Res. Appl. **39**(5), 442–451 (2014).
18. N. Moroney, M. D. Fairchild, R. W. G. Hunt, C. J. Li, M. R. Luo, and T. Newman, "The CIECAM02 color appearance model," in *10th Colour Imaging Conference (CIC)* (2002), pp. 23–27.
19. C. B. Barber, D. P. Dobkin, and H. T. Huhdanpaa, "The Quickhull algorithm for convex hulls," ACM Trans. Math. Softw. **22**(4), 469–483 (1996).
20. N. Moroney, "A comparison of the CIELAB and CIECAM97s," in *6th Colour Imaging Conference (CIC)* (1998), pp. 17–21.
21. C. J. Li, M. R. Luo, and R. W. G. Hunt, "A revision of the CIECAM97s model," Color Res. Appl. **25**(4), 260–266 (2000).
22. M. R. Luo and C. J. Li, *CIECAM02 and its associated colour spaces. Colorimetry: Understanding the CIE system*, (John Wiley & Sons, Inc., 2007), Chapter 11.
23. M. R. Luo, *The CIE 1997 colour appearance model: CIECAM97s. Colour Engineering: Achieving Device Independent Color*, (John Wiley & Sons, Inc., 2002), Chapter 4.
24. C. J. Li and M. R. Luo, "Testing the robustness of CIECAM02," Color Res. Appl. **30**(2), 99–106 (2005).
25. M. R. Luo, G. H. Cui, and C. J. Li, "Uniform colour spaces based on CIECAM02 colour appearance model," Color Res. Appl. **31**(4), 320–330 (2006).